PAPER

A methodology for extracting the electrical properties of human skin

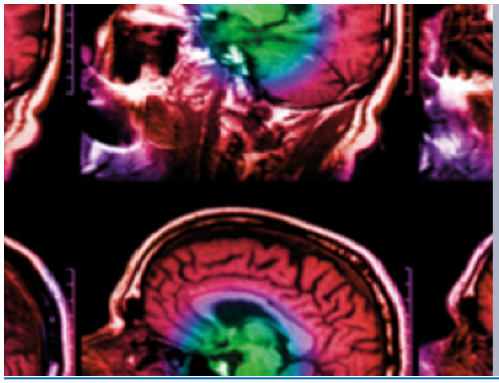

IOP Publishing Physiological Measurement

Physiol. Meas. **34** (2013) 723–736 doi:10.1088/0967-3334/34/6/723

A methodology for extracting the electrical properties of human skin

Ulrik Birgersson[1], Erik Birgersson[2], Ingrid Nicander[1] and Stig Ollmar[1]

[1] Department of Clinical Science, Intervention and Technology, Karolinska Institutet, Huddinge, Sweden
[2] Department of Chemical and Biomolecular Engineering, National University of Singapore, 5 Engineering Drive 2, Singapore 117576

E-mail: ulrik.birgersson@ki.se

Received 26 June 2012, accepted for publication 11 April 2013
Published 29 May 2013
Online at stacks.iop.org/PM/34/723

Abstract
A methodology to determine dielectrical properties of human skin is presented and analyzed. In short, it is based on a mathematical model that considers the local transport of charge in the various layers of the skin, which is coupled with impedance measurements of both stripped and intact skin, an automated code generator, and an optimization algorithm. New resistivity and permittivity values for the stratum corneum soaked with physiological saline solution for 1 min and the viable skin beneath are obtained and expressed as easily accessible functions. The methodology can be extended to account for different electrode designs as well as more physical phenomena that are relevant to electrical impedance measurements of skin and their interpretation.

Keywords: dermis, electrical impedance, epidermis, finite element, mathematical modeling, optimization

(Some figures may appear in colour only in the online journal)

1. Introduction

The human skin can be seen to comprise three main layers: epidermis, dermis and subcutis. The outer layer of the skin, the epidermis, is made up of five sub-layers with tightly packed cells. Its outermost sub-layer, the stratum corneum (SC), provides an effective barrier against chemicals and pathogens whilst limiting water loss through the skin. Underneath the epidermis lies the dermis with the main function to supply the epidermis with nutrients and provide mechanical strength and elasticity. This layer is mainly composed of collagen and elastin fibers and also contains sweat and sebaceous glands, hair follicles, sensory nerves, blood and lymph vessels. The innermost layer, the subcutis, consists mainly of fat and collagen cells and functions as an insulator and shock absorber (Agache and Humbert 2004).

One method to study human skin as well as to detect related skin alterations is electrical impedance spectroscopy, which allows for noninvasive measurements of the overall resistance and reactance of skin tissue at alternating current of various frequencies. In essence, the electrical impedance of intact skin is dominated by the SC at low frequencies ($\lesssim$ 1 kHz) and by the underlying layers at high frequencies ($\gtrsim$ 1 MHz) (Ackmann and Seitz 1984). Clinical changes can affect both the SC and the skin beneath in the form of for example skin irritations, or manifest themselves almost entirely below the SC, for example ageing, allergic reaction and early-stage skin cancer. It is therefore of interest to quantify the parameters governing the electrical behavior of the different skin layers in order to improve and optimize the electrode (EL) design and mode of operation as well as to better understand and interpret electrical impedance measurements.

The electrical properties of skin have previously been estimated by adjusting a tissue circuit equivalent to reflect the measured electrical impedance (Gabriel *et al* 1996, Yamamoto and Yamamoto 1976). The average resistivity and relative permittivity of skin were estimated by Yamamoto and Yamamoto (1976) after applying an 18% sodium chloride solution for 30 min before and after SC stripping, enabling the measurement of the SC and viable skin (VS) respectively. Later, Birgersson *et al* (2011) showed that the soaking time and sodium chloride concentration of the applied solvent significantly alter the electrical properties of the SC. Furthermore, they showed that Yamamoto and Yamamoto (1976) might have fallen short on the number of strippings necessary for complete removal of the SC, thus including part of the highly impedic nature of the SC into the electrical properties of the VS.

In view of the inherent complexity of the human skin and the lack of literature data for the electrical properties of skin, we introduce and validate a methodology that allows for efficient determination of the electrical properties of skin for arbitrary conditions (within limits). In short, the methodology is based on a mathematical model comprising conservation of charge in the functional layers of human skin with and without SC, as illustrated in figure 1; the model is solved numerically through automated model generation, and coupled with an optimization algorithm to minimize the difference between the predicted and experimentally measured impedance in order to secure the electrical material properties. New material properties in the form of easy-to-use functions for the electrical resistivity and relative permittivity of VS and SC on the volar forearm after soaking with a physiological saline solution (0.9% sodium chloride mass concentration) for 1 min are demonstrated. In this context, one inherent advantage of solving a local transport equation for charge throughout the various layers as opposed to solving a tissue-equivalent circuit-based model of the skin is that the former more closely resembles the actual physical phenomena. In addition, the model can easily be extended to account for additional physical phenomena, probe designs and local anomalies in the vicinity of the probe.

2. Materials and methods

The experimental impedance data in this study is taken from two separate sets of measurements, which were carried out after ethics approval and informed consent: the first is a study for SC stripping coupled with electrical impedance measurements, and the second is a study of electrical impedance variability between anatomical sites, race and ethnicity with the skin intact. The second study aims to test the feasibility of the obtained electrical properties from the first study.

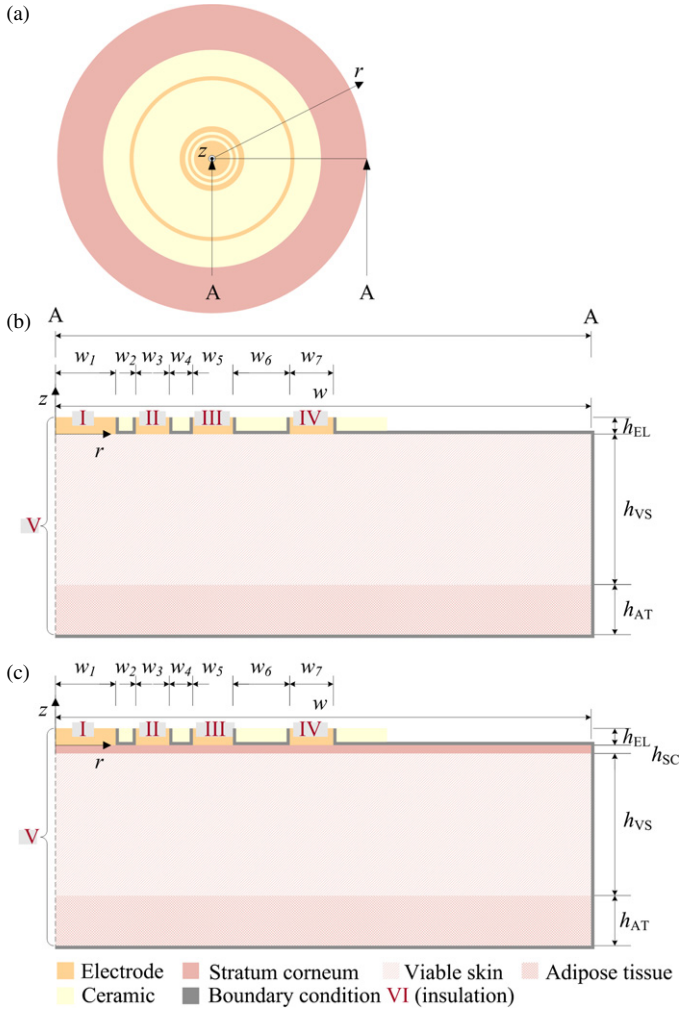

Figure 1. Schematic overview of the circular non-invasive EL applied on (a) skin, (b) VS and AT, and (c) stratum corneum, VS and AT. Length scales are shown for the different skin layers and ELs of the circular probe; boundary conditions for the mathematical model are given by roman numerals for easy identification: (I) sense EL, (II) guard EL, (III) secondary injection EL, (IV) primary injection EL, (V) symmetry axis and (VI) insulation. Dimensions are given in table 1.

2.1. Test subjects

In the first study, 26 healthy volunteers participated: 12 men and 14 women at 27 ± 6 years of age; they were non-smokers without any known skin diseases or allergies.

In the second study, 120 young volunteers participated: equal distribution of men and women at 24 ± 3 years of age; they were non-smokers without any known skin diseases or allergies; and on the day of the measurements they were asked to abstain from moisturizers.

2.2. Stratum-corneum stripping

A series of electrical impedance measurements with an in-house prototype of an electrical-impedance spectrometer and a noninvasive probe were performed on the volar forearm on

Table 1. Base-case model parameters.

Model objects	Acronym	Value	Unit
Current detection electrode	w_1	1	mm
Ceramic	w_2, w_4, w_6	0.15, 0.15, 1.9	mm
Guard Ring	w_3	0.3	mm
Secondary injection electrode	w_5	0.5	mm
Primary injection electrode	w_7	0.5	mm
Computational domain	w	7	mm
Electrode	h_{EL}	0.1	mm
Adipose tissue	h_{AT}	1.2	mm
Viable skin	h_{VS}	1.2	mm
Stratum corneum	h_{SC}	14	μm
Operating parameters			
Current penetration depth setting	α	0.1	–
Excitation voltage	V_0	50	mV

healthy subjects in 1996. Prior to measurements, the volunteers were positioned in a prone or supine position after which the skin was inundated with a physiological saline solution (0.9 % sodium chloride mass concentration) for 1 min. The physiological saline solution was applied to ensure that the contact resistance between the non-invasive probe and skin was kept to a minimum. The initial measurement on each subject was performed on intact skin followed by stripping of the SC with Scotch® Magic™ Cellulose Tape. Electrical impedance measurements were carried out after every fifth SC strip. The procedure was repeated until a total of 80 SC strippings had been performed. The relative air humidity was 24 ± 8 % and the ambient temperature was maintained at 21.9 ± 0.5 °C.

In addition, 3 mm punch biopsies were taken on four subjects before stripping, after 80 SC strippings and 1 week after stripping; the biopsies were assessed histologically for signs of inflammation and amount of remaining corneocyte layers.

The circular non-invasive EL consisted of a current detector, a guard ring and two voltage-injection ELs, as depicted in figure 1 (Nicander 1999). The in-house impedance-spectrometer prototype measured the impedance of the skin at 31 frequencies logarithmically distributed between 1 kHz and 1 MHz at five different current penetration depth settings; the latter were obtained by varying the applied voltage at the second injection EL (boundary III in figure 1(a)) from 5 to 50 mV. The electrical impedance measurements were subjected to electromagnetic disturbances detectable in the form of spikes; these were identified and removed with linear interpolation between neighboring points. In addition, the spectrometer had difficulties measuring in the lower frequency range ($\lesssim$ 10 kHz), which could be identified and corrected by replacing the phase of the electrical impedance measurement in the lower frequency range with the phase value obtained at 10 kHz. Finally, the measurements were filtered by means of a Savitsky–Golay smoothing filter with an 11-point window size and a polynomial order 2 (Savitzky and Golay 1964).

2.3. Intact skin

Electrical impedance measurements with a SciBase II impedance spectrometer and a non-invasive probe (Aberg 2004, SciBase 2012) were performed on the volar forearm of the volunteers in 2007. The skin was inundated with a physiological saline solution (0.9% sodium chloride mass concentration) for 1 min, after which the measurements were conducted. Similar to the aforementioned stripping study, the volunteers were placed in a prone or supine position.

The relative air humidity was 36 ± 7 %, and the ambient temperature was maintained at 21.7 ± 0.3 °C.

The SciBase II impedance spectrometer measured the impedance of the skin at 35 frequencies logarithmically distributed between 1.0 kHz and 2.5 MHz at five different current penetration depth settings, which are obtained by varying the applied voltage at the second injection EL (boundary III in figure 1(a)) from 5 to 50 mV. The non-invasive probe is similar in functionality and of the same design as the EL used in 1996.

2.4. Skin thickness

The variability of the skin thickness for the SC and VS is estimated from Birgersson *et al* (2011), who summarized existing literature on measurements of the skin thickness of the forearm for a female cohort with various techniques, and found the SC to be 14 μm $\pm$ 3 μm (mean $\pm$ standard deviation) and the VS to be 1.2 mm $\pm$ 0.2 mm. Since Birgersson *et al* (2011) only incorporated the female cohort (Egawa *et al* 2007, Egawa and Tagami 2008, Crowther *et al* 2008, Batisse *et al* 2002, Huzaira *et al* 2001, Hoffmann *et al* 1994, Seidenari *et al* 2000, Moore *et al* 2003, Sandby-Moller *et al* 2003, Holbrook and Odland 1974, Schwindt *et al* 1998, Pirot *et al* 1998, Tsai *et al* 2003), the thicknesses were re-evaluated to include both males and females. No significant differences in skin thickness were found between the cohort comprising both males and females and the cohort with only female subjects. The skin thickness variability estimates by Birgersson *et al* (2011) were therefore used for both calibration and verification purposes.

2.5. Mathematical model

We postulate that the skin can be modeled as a three-layer entity, comprising SC, VS consisting of the viable epidermis and dermis, and *adipose tissue* (AT); here, the living epidermis and dermis are incorporated into the VS, and subcutaneous fat into the AT. The electrical properties of the subcutaneous fat are assumed to correspond to the electrical properties of AT obtained by Gabriel *et al* (1996) and therefore only the electrical properties of the SC and VS are to be determined.

The gold-plated probe of the electrical impedance spectrometer with one sense, one guard and two injection ELs is circular (figure 1), whence we can reduce the three-dimensional domain to a two-dimensional, rotation-symmetric counterpart around the center of the probe and adjacent skin.

For later purposes, we distinguish between two cases: VS and AT for stripped skin (figure 1(b)); and SC, VS and AT for intact skin (figure 1(c)).

2.5.1. Governing equations. The mathematical model considers conservation of charge throughout the various skin layers in the frequency domain (Birgersson *et al* 2011):

$$\nabla \cdot \left[\left(\sigma^{(i)}(\nu) + j\omega\varepsilon_0 \varepsilon_r^{(i)}(\nu) \right) \nabla\phi \right] = 0, \tag{1}$$

where $\sigma^{(i)}(\nu)$ is the electric conductivity of layer i (i = SC, VS, AT, EL), which is a function of the applied frequency, ν; j is the imaginary number, ω is the angular frequency, ε_0 and $\varepsilon_r^{(i)}(\nu)$ are the relative permittivities of vacuum and the skin layer respectively, and ϕ is the electric potential. In general the material properties—electric conductivity and relative permittivity—are functions not only of the applied frequency but also of other factors such as soaking time and salt concentration; we only consider the frequency here for simplicity, but note that one could easily extend the methodology to map the material properties with respect to the other factors.

2.5.2. Boundary conditions. The following boundary conditions apply (see figure 1 for the placement of roman numerals):

- At the sense (I) and guard EL (II), we specify the ground potential:

$$\phi = 0. \tag{2}$$

The SciBase II impedance spectrometer with the non-invasive probe actively drives the ground EL to signal ground by use of an operation amplifier. Therefore, both the sense and ground ELs are at the same potential, i.e. 0 V, even though they are not short circuited.

- At the injection ELs (III and IV), we prescribe the following potentials:

$$\phi = \alpha V_0, \quad \text{(III)} \tag{3}$$

$$\phi = V_0, \quad \text{(IV)} \tag{4}$$

where α is a constant. Since the results for the electrical properties do not vary significantly between the different current penetration depth settings of the SciBase II impedance spectrometer nor for the prototype experimental data, the current penetration depth setting 5 was used; i.e., the second injection EL (III) is set to 5 mV ($\alpha = 0.1$) as the other 4 voltage settings give rise to similar behavior.

- At the symmetry axis (V) and the insulated boundaries (VI), we set no-flux conditions:

$$\mathbf{n} \cdot \mathbf{J} = 0, \tag{5}$$

where $\mathbf{n}$ is a vector normal to the boundary and $\mathbf{J} = -(\sigma^{(i)}(\nu) + j\omega\varepsilon_0\varepsilon_r^{(i)}(\nu))\nabla\phi$ is the total current density comprising both the conduction and displacement current density. The insulated boundaries (VI) either represent the interface between skin and air or the interface between the computational domain and adjacent skin, which is sufficiently far away from the probe that the currents there are negligible.

2.5.3. Constitutive relations. The functional form of the electric resistivity, $\rho^{(i)}(\nu) \equiv 1/\sigma^{(i)}(\nu)$, and relative permittivity of AT in the frequency range 1–10^3 kHz can be written as follows:

$$\rho^{(\mathrm{AT})} = 10^{1.7402}, \tag{6a}$$

$$\varepsilon_r^{(\mathrm{AT})}(\Omega) = 10^{-5.2423\times10^{-4}\Omega^5 - 4.0926\times10^{-4}\Omega^4 + 1.1797\times10^{-1}\Omega^3 - 7.7214\times10^{-1}\Omega^2 + 8.3142\times10^{-2}\Omega + 7.5844}, \tag{6b}$$

$$\Omega = \log_{10}(\nu). \tag{6c}$$

Essentially, these functions for the AT were created by fitting a fifth order polynomial to the measured tabularized data obtained from Gabriel *et al* (1996) in the frequency domain 1–10^3 kHz, with a view to minimize the coefficients and so secure a compact, simple form.

The predicted electrical impedance, Z_{mod}, is defined as

$$Z_{\mathrm{mod}} = \frac{V_0}{2\pi \int_0^{w_1} r\mathbf{n} \cdot \mathbf{J}\, \mathrm{d}r}, \tag{7}$$

where the denominator is the integral of the current density over the area of the innermost EL. (N.B.: $\mathbf{J}$ is complex-valued.)

2.6. Numerics

The commercial finite-element solver COMSOL MULTIPHYSICS 3.5a (COMSOL 2008) was employed to solve the complex-valued partial differential equation, equation (1), boundary conditions, equations (2)–(5), and constitutive relations, equations (6*a*)–(6*c*). In brief, the computational domains (figure 1(b) and (c)) were resolved with a mesh of around 10^5 triangular elements after mesh-independence tests; the direct solver UMFPACK was selected as the linear solver with a relative convergence tolerance of 10^{-6}; and a typical run for one frequency required around 2 sec (wall-clock time) with 10^4 degrees of freedom (quadratic Lagrange elements) on a 2.5 GHz workstation.

Optimization was carried out with the genetic-algorithm toolbox in Matlab (2011) to minimize the following fitness function:

$$f(Z_{\mathrm{mod}}, Z_{\mathrm{exp}}) = \frac{|\mathrm{Re}(Z_{\mathrm{mod}}) - \mathrm{Re}(Z_{\mathrm{exp}})| + |\mathrm{Im}(Z_{\mathrm{mod}}) - \mathrm{Im}(Z_{\mathrm{exp}})|}{|\mathrm{Re}(Z_{\mathrm{exp}})| + |\mathrm{Im}(Z_{\mathrm{exp}})|}; \tag{8}$$

iterations were carried out until $f(Z_{\mathrm{mod}}, Z_{\mathrm{exp}}) < 10^{-3}$ for every measured frequency with Z_{exp} denoting the experimentally measured impedance. Here, we chose a genetic algorithm since we found heuristically that it provided the best convergence behavior as compared to, e.g., gradient-based methods. Initial guesses for the to-be-determined material properties were taken from Birgersson *et al* (2011) .

In order to ensure a minimum of manual input for the optimization of the mathematical model to determine the electrical properties, we exploited the inherent two-way coupling between MATLAB and COMSOL; i.e., the mathematical model was implemented as a MATLAB script that manipulates a structure—with all the information pertaining to the numerical implementation of the partial differential equation, equation (1), as well as features such as geometry, mesh and solver parameters—generated by COMSOL. The script allows for automated code generation in that the code can receive information after which it reads in all operating, geometrical and physical parameters, draws and meshes the geometry, introduces the governing equation and constitutive relations, specifies the boundary conditions, solves the resulting set of equations, and postprocesses the results. This automated procedure thus allows for a significant reduction in computational complexity and time since no manual input is required.

We note that any commercial or in-house software could be employed provided that the integration of the three steps—numerical implementation of the mathematical model, automated code generation, and optimization—can be carried out without manual input to allow for fast and computationally efficient determination of the electrical material properties and their functional form.

2.7. Overview of the methodology

The herein proposed methodology rests on four pillars as illustrated in the flowchart in figure 2: experimental measurements, optimization, automated code generation, and a mathematical model. In essence, an optimization algorithm receives the electrical impedance from the experimental measurements, Z_{exp}, of an individual and provides estimates for the electrical parameters that are to be determined to the automated code generator; the latter, in turn, returns Z_{mod} to the optimization algorithm, which iterates until the fitness function has reached a certain tolerance. An outer for-loop then works through the measured frequency domain from 1 to 10^3 kHz for each individual. This procedure was then repeated for 26 and 120 individual measurements in the first and second study respectively. Finally, the median properties were calculated since the distributions for the two studies were not normally distributed.

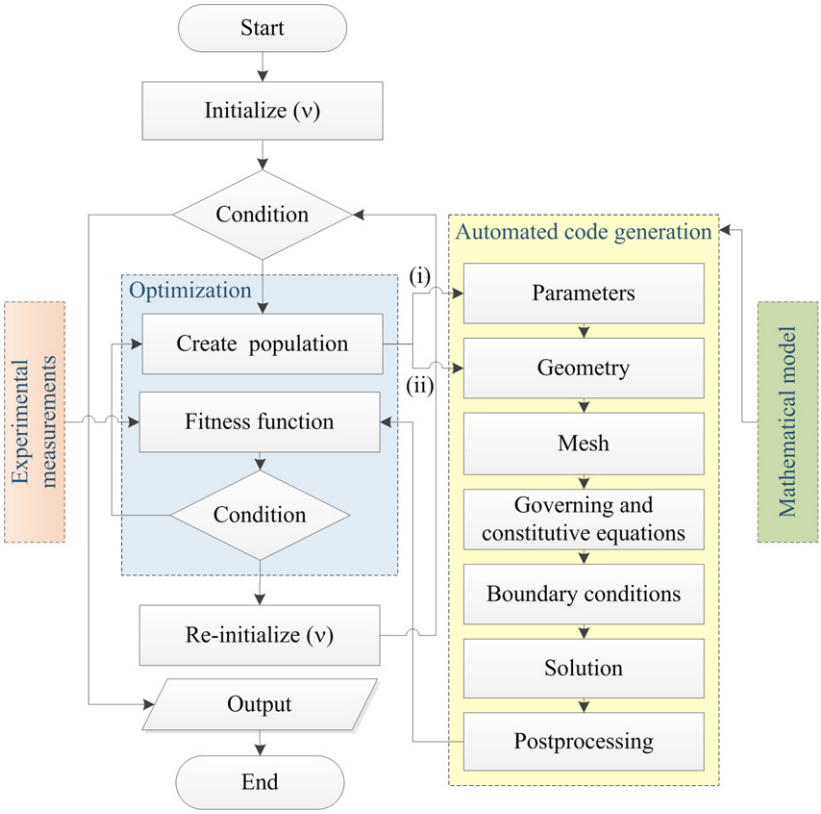

Figure 2. Flowchart of the methodology—an optimization algorithm receives the electrical impedance from the experimental measurements, Z_{exp}, of an individual at the given initialized ν and provides estimates for the electrical parameters that are to be determined to the automated code generator; the latter, in turn, returns Z_{mod} to the optimization algorithm, which iterates until the fitness function has reached a certain tolerance (optimization condition). An outer for-loop then works through the measured frequency domain from 1 to 10^3 kHz for each individual (outer-for-loop-condition).

Furthermore, we started with the electrical impedance measurements obtained after SC strippings in order to decouple the electrical properties of the viable skin and the SC. The average electrical properties of the VS were calculated with the geometry illustrated in figure 1(b) by setting the thickness of the VS, h_{VS}, and subcutaneous fat, h_{AT}, to the mean population thickness of 1.2 mm respectively. Once the functional forms for the average permittivity and resistivity of the VS were secured, we proceeded with the measurements of intact skin. The average electrical properties of the SC were calculated with the geometry illustrated in figure 1(c) by setting the thickness of the VS, h_{VS}, subcutaneous fat, h_{AT}, and SC, h_{SC}, to the mean population thicknesses of 1.2 mm, 1.2 mm and 14 μm, respectively.

3. Results

The calculated values for the resistivity and relative permittivity from the first study of VS and SC inundated with sodium chloride mass concentration of 0.9% for 1 min and the values by Yamamoto and Yamamoto (1976) and Birgersson *et al* (2011) are shown in figures 3(a) and (b).

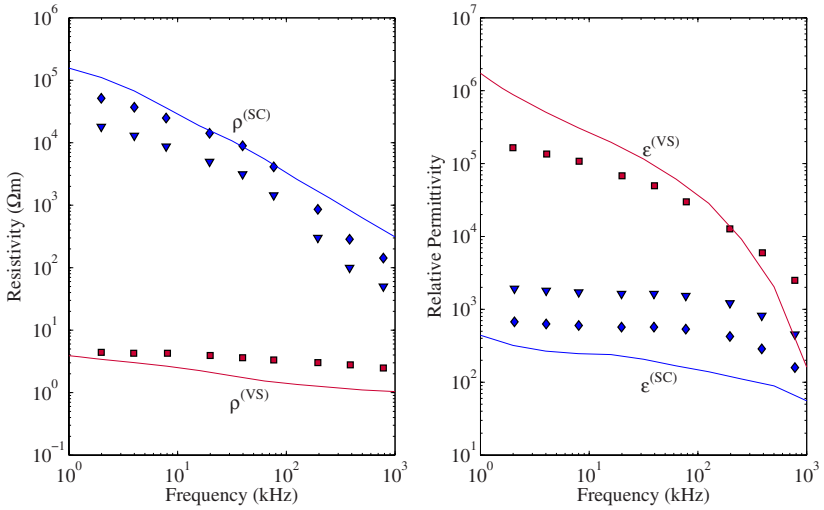

Figure 3. (a) Resistivity and (b) relative permittivity of VS and stratum corneum by Yamamoto and Yamamoto (1976) (■), Birgersson *et al* (2011) (♦) and calculated median values (−).

Out of the 26 electrical impedance measurements on stripped skin, two outliers could be identified. The electrical impedance was 15 and 50 kΩ at 1 kHz and showed no signs of double dispersion (Serup *et al* 2006), clearly indicating that a significant amount of SC still remained. The two measurements were thus excluded prior to calculating the material properties.

For the second study the median electrical properties of the VS from the SC stripping study was employed to determine the resistivity and permittivity of the SC. Two outliers—out of the 120 measurements—were identified in the electrical impedance data and removed. The deviating electrical impedance of the outliers can be explained by a poor galvanic contact between the EL and skin, clearly discernible in the impedance spectra (not shown here). The calculated median values for the resistivity and relative permittivity for the SC for both studies (inundated with sodium chloride mass concentration of 0.9% for 1 min) and their relative errors are depicted in figure 4. The relative errors are defined as $\left|\rho^{(\mathrm{SC})}_{\text{second study}} - \rho^{(\mathrm{SC})}_{\text{first study}}\right| / \rho^{(\mathrm{SC})}_{\text{second study}}$ and $\left|\varepsilon^{(\mathrm{SC})}_{\text{second study}} - \varepsilon^{(\mathrm{SC})}_{\text{first study}}\right| / \varepsilon^{(\mathrm{SC})}_{\text{second study}}$.

The median electrical properties of the VS and of the SC in the frequency range 1–10^3 kHz, obtained from the first and second study respectively, can conveniently be written as exponential functions in log space:

$$\rho^{(\mathrm{SC})}(\Omega) = 10^{1.1516\times10^{-2}\Omega^5 - 2.5509\times10^{-1}\Omega^4 + 2.2537\Omega^3 - 9.9955\Omega^2 + 21.404\Omega - 11.803}, \tag{9a}$$

$$\varepsilon_r^{(\mathrm{SC})}(\Omega) = 10^{-1.1319\times10^{-2}\Omega^5 + 2.3953\times10^{-1}\Omega^4 - 2.0255\Omega^3 + 8.5278\Omega^2 - 17.961\Omega + 17.570}, \tag{9b}$$

$$\rho^{(\mathrm{VS})}(\Omega) = 10^{-1.5178\times10^{-2}\Omega^5 + 3.4167\times10^{-1}\Omega^4 - 3.0088\Omega^3 + 12.952\Omega^2 - 27.471\Omega + 23.688}, \tag{9c}$$

$$\varepsilon_r^{(\mathrm{VS})}(\Omega) = 10^{-4.4465\times10^{-2}\Omega^5 + 9.2429\times10^{-1}\Omega^4 - 7.7649\Omega^3 + 32.847\Omega^2 - 70.466\Omega + 67.610}. \tag{9d}$$

These functions are illustrated in figure 5 together with the population variability as 25/50/75 percentiles and upper and lower ranges based on the 1.5 interquartile range rule (equivalent to the boxplot for discrete data; the 50 percentile corresponds to the median).

The biopsies in the first study showed that no initial inflammatory response occurred within the time frame for stripping and impedance measurements.

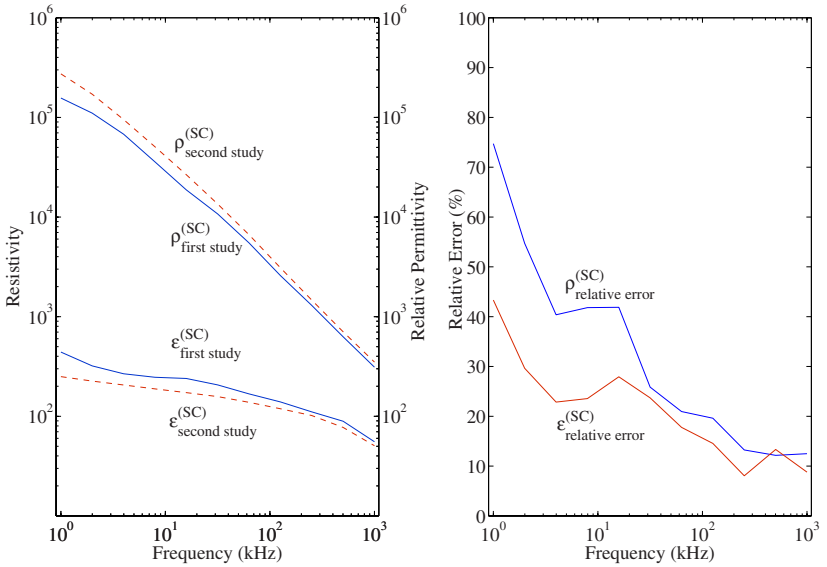

Figure 4. (a) Median resistivity and relative permittivity of the stratum corneum for the first (−) and second study (−−) and (b) their relative errors.

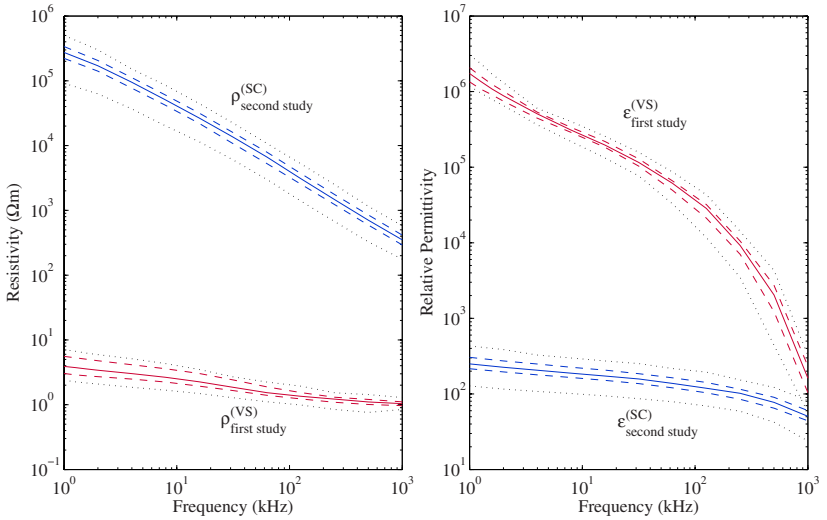

Figure 5. (a) Resistivity and (b) relative permittivity of VS and stratum corneum with lower/upper whiskers based on the 1.5 interquartile range (· · ·), 25/75th percentiles (−−) and median (−).

The derived median material properties given by equations (6*a*), (6*b*) and (9*a*)–(9*d*) for AT, VS and SC were then applied in the mathematical model illustrated in figure 1(c) to elucidate the variability in a given population. Three skin thickness cases were implemented and compared with measurements (see figure 6): $h_{SC} = 14\ \mu$m, $h_{VS} = 1.2$ mm; $h_{SC} = 20\ \mu$m, $h_{VS} = 0.8$ mm; and $h_{SC} = 8\ \mu$m, $h_{VS} = 1.6$ mm whilst the adipose layer h_{AT} is kept constant at 1.2 mm. The skin thicknesses were chosen from section 2.4, as they encompasses 95% of the normal skin thickness variability in a given population.

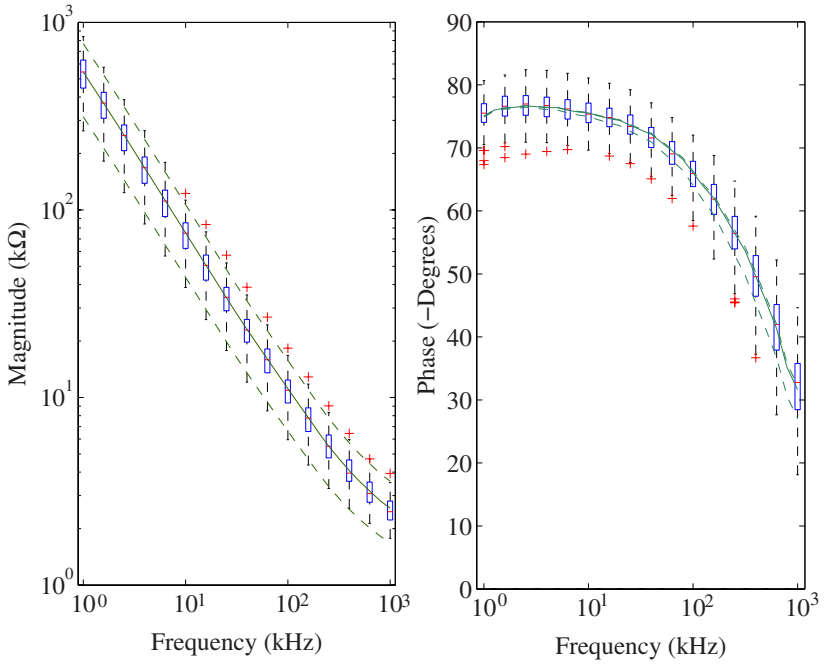

Figure 6. Box plot of the experimental measurements and model predictions based on calculated electrical properties of the SC and VS with (−−) 8 μm SC and 1.6 mm VS, (−) 14 μm SC and 1.2 mm VS; and (−−) 20 μm SC and 0.8 mm with a 1.2 mm thick adipose layer for (a) the magnitude and (b) the phase.

4. Discussion

By applying our methodology to the first study with 26 volunteers, we have secured new average electrical properties of both the SC and VS, which had been soaked with a physiological saline solution for 1 min, as can inferred from figure 3. Moving on to the second study (see figure 4) it is clear that the calibrated electrical properties of the SC only agree above 100 kHz where the relative error remains below 20%. The reason for the increasing disagreement as the frequency approaches the lower bound of 1 kHz can be found in the fact that the first study was carried out with an in-house prototype, which was found to be less accurate in the lower frequency range ($\nu \lesssim 10$ kHz) for external loads exceeding $\sim$200 kΩ. Since the measured electrical impedance of stripped skin never exceeds 10 kΩ, the calibrated values for the resistivity and relative permittivity for VS are not affected in the same manner. Thus, the median material properties of the VS derived from the stripping study and the SC calibrated from the second study should be used, as illustrated in figure 5.

As can be inferred from figure 6, the new median electrical properties in conjunction with the skin thickness variability found in literature are able to capture the variability of the measured electrical impedance in the studied population.

To ensure that an inflammatory response due to skin stripping would not alter the measured electrical impedance, biopsies were taken directly after measurements had been taken on stripped skin. The results from the biopsies show that the initial inflammatory response did not occur in the time frame of the stripping procedure; and even though the skin exhibited a visual redness, one does not need to take this into account when the VS electrical properties

are determined. The stripping procedure as such is therefore a good experimental approach for extracting the electrical properties of the VS, because it appears to be undistorted by the stripping procedure.

It is common to find the electrical properties of tissue in the form of figures or tabulated data, which not only limits the accuracy as values have to be extracted manually and/or interpolated but is also rather 'tedious' . Therefore, the electrical properties are given in a functional form, equations (6*a*), (6*b*) and (9*a*)–(9*d*), providing easy access in the frequency range 1–10^3 kHz. The functional form has been chosen to provide a compact notation with a minimal number of coefficients whilst still ensuring a sufficiently high accuracy. One can also reduce the order of the polynomials if a smaller range of frequencies is of interest.

Finally, we note that the underlying mathematical model for the charge transport in the skin can be extended in several directions:

- *Electrode design*. The automated code generation can easily create different types of ELs (see arrow (ii) in figure 2): e.g., rectangular ELs with/without spikes and with more/less ELs. One can then study the bioimpedance and variations thereof related to EL design. In this context, the model can provide information such as the current pathways in the various layers of the skin at different frequencies. Further, one could even aim to carry out optimization of the EL design itself with a view to, e.g., capture clinical changes more accurately.
- *Physical phenomena*. The model is based on continuum physics and can easily be extended with differential equations to account for additional phenomena that occur during measurements. One such example is the mechanical deformation of the skin that occurs when the probe is pressed against the skin during measurements; see, e.g., Agache *et al* (1980). The deformation can be added by solving a partial differential equation for the deformation in the skin and coupling the deformation with the charge transport; coupling could be carried out with an arbitrary Lagrangian–Eulerian formulation. Another phenomena could be the water gradient that is known to exist in the skin (Egawa and Tagami 2008). Most importantly, and as alluded to in the *introduction*, the mathematical model presented here thus has an advantage vis-à-vis electric-circuit based models.
- *Spatial resolution*. More information of the structures that can be found in the three layers we consider here could be added to increase the spatial resolution. One could for this purpose add the distinct layers that can be found in the SC that were recently visualized by Iwai *et al* (2012) or add cellular information (Walker *et al* 2002, 2003, 2005, Jones *et al* 2003, Keshtkar *et al* 2006, Hartinger *et al* 2009).
- *Model reductions.* At 1–100 kHz, Birgersson *et al* (2012) have shown that the mathematical model can be completely reduced to analytical closed-form expressions for the magnitude, phase, electrical properties and SC thickness. This significantly simplifies the methodology in this frequency range since numerical solutions are no longer necessary.
- *Clinical changes*. The resistivities and permittivities of the SC and VS clearly show that the electrical properties of skin are governed, even to a larger extent than previously shown (Ackmann and Seitz 1984, Martinsen *et al* 1999), by the SC. This, in turn, implies that at frequencies below and around 1 kHz, the measured electrical impedance with a flat-EL design will almost only detect changes that are SC related, such as changes in the barrier function or compositional changes. The contribution of the SC to the measured electrical impedance even in the higher frequencies, $\sim 10^3$ kHz, is also not negligible. Therefore, if one aims to quantify changes that occur almost entirely underneath the SC—such as early-onset skin cancers and ageing phenomena coupled with collagen degradation—the electrical impedance of the SC clearly needs to be reduced. Reducing the impact of the

SC could be accomplished non-invasively by an increase of the measurement frequency, application of topical gels/creams/pastes, furnishing the ELs with spikes, by utilizing a four-point measurement technique or invasively by methods such as skin stripping or other forms of mechanical of chemical abrasion.

5. Conclusions

A methodology—based on experimental impedance measurements, a mathematical model comprising conservation of charge in the functional layers of human skin coupled with automated code generation and an optimization algorithm—has been developed and verified experimentally. New resistivity and permittivity values for viable skin and stratum corneum soaked with a physiological saline solution for 1 min on the volar forearm have been obtained and expressed as easily accessible functions.

The presented methodology can be extended to encompass other types of tissue, soaking time, and different solvents, which in turn allows for extraction of new electrical material properties as well as analysis of the current and voltage distributions. In addition, we have discussed other extensions such as electrode design, coupled physical phenomena such as deformation of the skin during impedance, resolution of the skin and clinical changes that could be studied.

References

Aberg P 2004 Skin cancer as seen by electrical impedance *PhD Thesis* Karolinska Institutet, Stockholm, Sweden (available at http://diss.kib.ki.se/2004/91-7140-103-2/thesis.pdf)

Ackmann J J and Seitz M A 1984 Methods of complex impedance measurements in biologic tissue *Crit. Rev. Biomed. Eng.* **11** 281–311 PMID: 6391815

Agache P and Humbert P (ed) 2004 *Measuring the Skin: Non-invasive Investigations, Physiology, Normal Constants* 1st edn (Berlin: Springer)

Agache P, Monneur C, Leveque J and Rigal J 1980 Mechanical properties and Young's modulus of human skin *in vivo Arch. Dermatol. Res.* **269** 221–32

Batisse D, Bazin R, Baldeweck T, Querleux B and Leveque J-L 2002 Influence of age on the wrinkling capacities of skin *Skin Res. Technol.* **8** 148–54

Birgersson U, Birgersson E, Åberg P, Nicander I and Ollmar S 2011 Non-invasive bioimpedance of intact skin: mathematical modeling and experiments *Physiol. Meas.* **32** 1–18

Birgersson U, Birgersson E and Ollmar S 2012 Estimating electrical properties and the thickness of skin with electrical impedance spectroscopy: mathematical analysis and measurements *J. Electr. Bioimpedance* **3** 51–60 (available at www.journals.uio.no/index.php/bioimpedance/article/view/400)

COMSOL 2008 COMSOL Multiphysics 3.5a (available at http://www.comsol.com)

Crowther J M, Sieg A, Blenkiron P, Marcott C, Matts P J, Kaczvinsky J R and Rawlings A V 2008 Measuring the effects of topical moisturizers on changes in stratum corneum thickness, water gradients and hydration *in vivo Br. J. Dermatol.* **159** 567–77

Egawa M, Hirao T and Takahashi M 2007 *In vivo* estimation of stratum corneum thickness from water concentration profiles obtained with raman spectroscopy *Acta Dermatol. Venereol.* **87** 4–8

Egawa M and Tagami H 2008 Comparison of the depth profiles of water and water-binding substances in the stratum corneum determined *in vivo* by raman spectroscopy between the cheek and volar forearm skin: effects of age, seasonal changes and artificial forced hydration *Br. J. Dermatol.* **158** 251–60

Gabriel C, Gabriel S and Corhout E 1996 The dielectric properties of biological tissue. I: literature survey *Phys. Med. Biol.* **41** 2231–49

Gabriel S, Lau R W and Gabriel C 1996 The dielectric properties of biological tissue. II: measurements in the frequency range 10 Hz to 20 GHz *Phys. Med. Biol.* **41** 2251–69

Hartinger A E, Guardo R, Kokta V and Gagnon H 2009 A 3d hybrid finite element model to characterize the electrical behavior of cutaneous tissues *IEEE Trans. Biomed. Eng.* **57** 780–9

Hoffmann K, Stücker M, Dirschka T, Görtz S, Al-Gammal S, Dirting K, Hoffmann A and Altmeyer P 1994 Twenty MHz b-scan sonography for visualization and skin thickness measurement of human skin *J. Eur. Acad. Dermatol. Venereol.* **3** 302–13

Holbrook K and Odland G 1974 Regional differences in the thickness (cell layers) of the human stratum corneum: an ultrastructral analysis *J. Invest. Dermatol.* **62** 415–22

Huzaira M, Rius F, Rajadhyaksha M, Anderson R R and Gonzáles S 2001 Topographic variations in normal skin, as viewed by *in vivo* reflectance confocal microscopy *J. Invest. Dermatol.* **116** 846–52

Iwai I *et al* 2012 The human skin barrier is organized as stacked bilayers of fully extended ceramides with cholesterol molecules associated with the ceramide sphingoid moiety *J. Invest. Dermatol.* **132** 2215–25

Jones D M, Smallwood R H, Hose D R, Brown B H and Walker D C 2003 Modelling of epithelial tissue impedance measured using three different design of probe *Physiol. Meas.* **24** 605–23

Keshtkar A, Keshtkar A and Smallwood R H 2006 Electrical impedance spectroscopy and the diagnosis of bladder pathology *Physiol. Meas.* **27** 586–96

Martinsen O G, Grimnes S and Haug E 1999 Measuring depth depends on frequency in electrical skin impedance measurements *Skin Res. Technol.* **5** 179–81

Matlab 2011 www.mathworks.com

Moore T L, Lunt M, McManus B, Anderson M E and Herrick A L 2003 Seventeen-point dermal ultrasound scoring system—a reliable measure of skin thickness in patients with systemic sclerosis *Rheumatology* **42** 1559–63

Nicander I 1999 Electrical impedance related to experimentally induced changes of human skin and oral mucosa *PhD Thesis* Karolinska Institutet, Stockholm, Sweden

Pirot F, Berardesca E, Kalia Y N, Singh M, Maibach H I and Guy R H 1998 Stratum corneum thickness and apparent water diffusivity: facile and noninvasive quantitation *in vivo Pharm. Res.* **15** 492–4

Sandby-Moller J, Poulsen T and Wulf H C 2003 Epidermal thickness at different body sites: relationship to age, gender, pigmentation, blood content, skin type and smoking habits *Acta Dermatol. Venereol.* **83** 410–3

Savitzky A and Golay M J E 1964 Smoothing and differentiation of data by simplified least squares procedures *Anal. Chem.* **36** 1627–39

Schwindt D A, Wilhelm K P and Maibach H I 1998 Water diffusion characteristics of human stratum corneum at different anatomical sites *in vivo J. Invest. Dermatol.* **111** 385–9

SciBase 2012 SciBase AB homepage (www.scibase.se)

Seidenari S, Giusti G, Bertoni L, Magnoni C and Pellacani G 2000 Thickness and echogenicity of the skin in children assessed by 20-MHz ultrasound *Dermatology* **201** 218–22

Serup J, Jemec G B E and Grove G L (ed) 2006 *Handbook of Non-Invasive Methods and the Skin* 2nd edn (Boca Raton, FL: CRC / Taylor and Francis)

Tsai J-C, Lin C-Y, Sheu H-M, Lo Y-L and Huang Y-H 2003 Noninvasive characterization of regional variation in drug transport into human stratum corneum *in vivo Pharma. Res.* **20** 632–8

Walker D C, Brown B H, Blackett A D, Tidy J and Smallwood R H 2003 A study of the morphological parameters of cervical squamous epithelium *Physiol. Meas.* **24** 121–35

Walker D C, Brown B H, Smallwood R H, Hose D R and Jones D M 2002 Modelled current distribution in cervical squamous *Physiol. Meas.* **23** 159–68

Walker D C, Brown B H, Smallwood R H, Hose D R and Jones D M 2005 Modelling the electrical properties of bladder tissue—quantifying impedance changes due to inflammation and oedema *Physiol. Meas.* **26** 251–68

Yamamoto T and Yamamoto Y 1976 Dielectric constant and resistivity of the epidermal stratum corneum *Med. Biol. Eng.* **14** 494–500